Environ Sci Pollut Res
DOI 10.1007/s11356-016-7366-x

SPATIAL AND TEMPORAL PATTERNS OF ANTHROPOGENIC INFLUENCE IN A LARGE RIVER BASIN. A MULTIDISCIPLINARY APPROACH

Evaluation and localization of an artificial drainage network by 3D time-lapse electrical resistivity tomography

T Jouen[1] · R Clément[1] · H Henine[1] · C Chaumont[1] · B Vincent[1] · J Tournebize[1]

Received: 4 March 2016 / Accepted: 1 August 2016

Abstract In France, 10 % of total arable land is equipped with subsurface drainage systems, to control winter and spring waterlogging due to a temporary perched water table. Most of these systems were installed in the1980s and have aged since then and may now need maintenance. Sometimes, the location of the systems is known, but the standard situation in France is that the original as-built master sketches are no longer available. Performance assessment of drainage systems and curative actions are complicated since drain location is unknown. In this article, the authors test the application of a non-destructive drain detection method which consists in water injection at the outfall of the drainage network combined with time-lapse electrical resistivity tomography (ERT) monitoring. To assess the performance of this methodology, which consists in measuring electrical resistivity from electrodes placed at the nodes of a 1.2-m regular mesh, the authors interpreted the signal using a two-step approach. The first step is based on 3D ERT numerical modelling during a scenario of surface infiltration processes (forward modelling followed by geophysical inversion); this step optimizes the ERT method for locating the infiltration at depths below 1 m. The second step is the validation of the results obtained by numerical modelling with an experimental data set, using water injection into the drainage network combined with time-lapse ERT monitoring on an experimental field site. The results showed the relevance of time-lapse ERT monitoring on a small agricultural plot for locating the drainage network. The numerical results also showed several limitations of the combined methodology: (i) it is necessary to use an electrode spacing unit less than 1.20 m, which does not facilitate investigation on large agriculture plots, (ii) measurements must be taken when resistivity contrast is the strongest between the infiltration area and the soil and (iii) the volume of water needed for injection can limit the extension of the method.

Keywords Electrical resistivity tomography · Time lapse · Drainage network

Responsible editor: Philippe Garrigues

✉ T Jouen
thomas.jouen@irstea.fr

[1] IRSTEA, Hydrosystems and Bioprocesses Antony, HBAN, 1 rue Pierre Gilles de Gennes, 10030Cedex, 92761 Antony, CS, France

Introduction

In France, the main goal of artificially drained waterlogged soil (about 10 % of arable land in France and 80 % of the Paris basin) is to remove excess water from the soil to the surface arterial water body network (Lesaffre, 1989; Zimmer et al., 1995). A drainage system in France consists of perforated or nested pipes connected to an arborescence of collectors which outfall to the arterial drainage system. Drain depth is typically 0.8 m, ranging from 0.8 to 1.2 m (Lesaffre, 1989) in accordance with the depth of the semi-impervious layer on which the small perched water table forms. Drains are spaced every 8–20 m (typically 10 m) using two types of pipes: (i) corrugated perforated PVC drains (two standardized inner/outer diameters: 44/50 mm or 58/65 mm) and (ii) pottery tiles (as in this study: 30/40 mm and 30 cm long).

These drainage systems need to be improved on many soils for sustainable agricultural production. The installation of this system causes an increase of the soil's water storage capacity, restoring infiltration capacity and, consequently, decreasing the surface runoff (Henine et al., 2010; Skaggs et al., 1994).

Published online: 26 August 2016

In France, the major national agricultural drainage networks were installed in the 1980s (Lagacherie, 1987). Today, the artificial drainage network has aged, and in several cases, the position of the drain is unknown because the historical drainage network cartography has been lost, destroyed or never existed.

Detecting the drain position is required when the water law is applied (i) to facilitate operation maintenance in order to position non-functioning drains and to avoid destructive investigation by back hoes or mechanical shovels and (ii) to assess the influence of current tile drainage on pre-existing wetlands, which are protected by the French water law. Our idea is to inject water in the drains in the dry season and to observe the rehydration of the soil around the drain using a geophysical method. Several publications in the geophysical literature have studied this issue (Allred et al., 2005, 2004; Cazorzi et al., 2013; Chow and Rees, 1989; Mathé and Lévêque, 2003); conversely, few articles have assessed the effectiveness of the drainage network (Allred and Redman, 2010). Several authors have demonstrated the ability of the cesium magnetometer to locate a drain (22 cm in diameter) with a horizontal accuracy of ±25 cm (Rogers et al., 2005; Mathé and Lévêque, 2003). However, this method is limited by the type of soil and its magnetic properties.

Allred et al. (2004) have tested four different geophysical methods for locating drain pipes with a diameter of 100 mm buried 0.4 m deep. For three of the four methods (geomagnetic, frequency domain electromagnetic and the electrical resistivity tomography [ERT] method), the authors reported that they provide good information on the spatial variation of soil properties around the drainage pipes. Indeed, the drainage installation modified the soil structure around the pipes. In contrast, only ground-penetrating radar (GPR) prospecting appears to be a suitable method for locating buried pipes with diameter greater than 100 mm. On all 11 field areas investigated by Allred et al. (2004) in the USA, GPR located 80 % of the pipes buried 1 m deep in several soil types. The optimization of this method (Allred et al., 2005) detected drain pipes with a diameter as small as 60 mm buried 1 m deep. The GPR method has been validated for locating buried drainage pipe and determining the pipe clogging state (Allred and Redman, 2010; Allred et al., 2005). However, only drains with diameters greater than 100 mm are available in the USA and Canada as a standard dimension. In France, agricultural plots were equipped with drainage pipe with an outer diameter of 60 mm buried at a depth of 1 m. GPR, radio magnetotellurics and thermography were tested, but the methods gave no significant results for detecting drainage pipes (Caul-Futy, 1994). According to the authors, these methods reach their limits when detecting small diameters (less than 50 mm) and very low soil electrical resistivity (less than 100 Ω.m). The literature also reports the use of remote sensing (high-resolution aerial photograph) for the location of buried drains (Naz et al., 2009). However, these techniques are used for large agricultural lands (several hundred km^2) and are limited when plant cover is abundant. The objective of this paper is to propose a new methodology based on geophysical measurement to locate small drainage networks (with drain diameters less than 60 mm).

Among the geophysical methods, ERT is widely used for environmental or agricultural needs (Benson, 1997; Clément et al., 2010; Michot, 2003; Samouëlian et al., 2005). The reconstruction of the distribution of electrical resistivity analyses complex 3D geometry of the soil structure or water content variation (Audebert et al., 2014). It is known that the use of ERT cannot detect and localize the drainage pipe directly because the drain pipe diameter is too small.

However, ERT used in time-lapse monitoring has become a reference tool in environmental applications (Barker and Moore, 1998; Brunet et al., 2010; Clément et al., 2009; Descloitres et al., 2008). Time-lapse monitoring consists of taking the same ERT measurement several times in the same place, namely before, during and after the hydrological processes are studied (Loke, 2000). Time-lapse electrical resistivity monitoring can study the leachate injection phenomena in waste landfill (Audebert et al., 2014; Clément et al., 2010, 2009; Moreau et al., 2003), evaluate soil infiltration (Brunet et al., 2010; Chaudhuri et al., 2013) and study the contamination of groundwater resources (Benson, 1997). In a recent article, Clement et al. (2014) demonstrated that time-lapse ERT could be used to characterize the seasonal infiltration at the field scale, for an agricultural plot equipped with a tile drainage network. The authors also assert that the variations of water content due to the drained pipe during the wet season are on the order of 2 or 3 % after a runoff episode. These variations are not sufficient to create sufficiently strong resistivity contrasts to locate drained pipes after a rainfall event. This paper investigates and evaluates the use of time-lapse ERT during water injection into the drainage system in order to characterize water fluxes and assess pipe functioning. In this experiment, this injection created an infiltration that can be followed with time-lapse ERT. The main assumption is based on the resistivity contrast created by sufficiently strong water injection, and then the locations of wet areas correspond to the location of drains.

Material and methods

General methodology

Therefore, the idea is to use the drainage pipes as an injection system and to monitor the variations of soil electrical resistivity using time-lapse ERT, to interpret changes within time and space in terms of water content in order to observe the spatial structure of these changes that could be related do drain positions. The electrical resistivity of a soil is influenced by several variables such as the texture, structure, porosity and the physical parameters of the soil depending on the water content, the temperature and the concentration of the soil solution (Archie, 1942; Michot, 2003; Samouëlian et al., 2005). If we assume that the variation of temperature and the electrical resistivity of the porous water are low during an experiment lasting 2 or 3 days, and if other soil parameters (such as soil porosity and texture) are stable, we can consider that the most influential parameter on the variation of the electrical resistivity is the water content variation. Recognizing that the ERT measurement is sensitive to the variation in water content allows us to localize the infiltration profile due to the injection of water and then to locate the drainage network. To evaluate the use of 2D or 3D ERT measurements in locating infiltration around drains between the soil surface and 1 m deep, we used the following general approach composed of two parts. (i) The first part involves the numerical optimization of the ERT method for locating infiltration at depths below 1 m. We use a classic approach applied in several papers (Clément et al., 2009; Radulescu et al., 2007; Yang, 2005) using ERT numerical modelling. This part is based on three steps. The first step consists in designing resistivity models corresponding to multiple realistic infiltration scenarios. The second step produces synthetic apparent resistivity data sets using a forward calculation Matlab script called F3DM (Forward 3D Modelling) combined with the finite element software Comsol Multiphysics (Clement et al., 2011). The third step is the inversion of the synthetic apparent resistivity data sets performed using the BERT software package (Günther and Rücker, 2011; Günther, 2004; Günther et al., 2006; Rücker et al., 2006) with common inversion parameters to obtain a calculated resistivity distribution. (ii) The second part validates the proposed methodology on a field application considering the numerical results from the first part.

Synthetic 3D models

Realistic infiltration scenarios were considered. If we assume that each drain is made of short 30-cm lengths of clay tiles placed end to end, then the infiltration will first evolve locally at the joints between two tiles. All infiltrations will then merge to form an infiltration lobe surrounding the entire drain. Since each tile is 30 cm long, it is assumed that ERT will only be able to detect the infiltration lobe and not the local point at the tile junctions. The infiltration area is considered to be more conductive than the soil unaffected by infiltration. This comes from a previous measurement campaign (Clément et al., 2014), which determined that the average resistivity of the area during the driest period of the year was 32 Ω.m, and the average resistivity of the infiltration area was 22 Ω.m. For these reasons, infiltration areas are represented by a parallelepiped (green, Fig. 1) with a bulk resistivity of 22 Ω.m. The model's structure before the injection phase is also represented by a rectangle parallelepiped measuring 30 m × 20 m × 10 m (blue, Fig. 1) with a bulk resistivity of 32 Ω.m. Six lines of 16 electrodes were placed for each of the synthetic models and are represented in Fig. 1 by a black dot. The positions of the electrodes and infiltrations on our models are similar to the field measurements (see section 2.2).

To produce different models, we varied the electrical resistivity ratio defined as the electrical resistivity after injection divided by the electrical resistivity before injection. The minimum bulk resistivity ratio possible to measure in the field was therefore 22/32 (0.6875). In our models, we decreased the resistivity contrast by decreasing the area resistivity. While varying the area's resistivity, we simulated ERT measurements on a more or less water-saturated soil.

To determine the ERT sensitivity to detecting an infiltration on a shallow surface, an experimental design was completed and allowed to build 27 infiltration scenario models. Three parameters were included in the experimental design:

- The infiltration width represented in Fig. 1 by the variable W.
- The infiltration thickness represented in Fig. 1 by the variable T.
- The bulk resistivity ratio represented in Fig. 1 by the variable R.

The set of values of the different variables of the infiltration geometry is presented in Table 1.

Forward modelling

Numerical tools

To estimate the apparent resistivity of our synthetic models, we chose to use Comsol Multiphysics, which is commonly used in geophysics modelling and presents a number of advantages (Bauer-Gottwein et al., 2010; Braun and Yaramanci, 2008; Clement et al., 2011). Electric field distribution can be modelled on a full 3D geometry using the AC/DC module (quasi-stationary electromagnetic field with the electromagnetic field theory) to evaluate the potential difference (ΔV_{MN}) induced by the injected electric current (I). To simulate the electric current injection with Comsol Multiphysics, intensity I of 1 A was injected into the two current electrodes, with the 3D model designed. At the end of the simulation, the potential differences ΔV_{MN} between the two potential electrodes were computed. Finally, apparent resistivity can be estimated using geometrical factor K,

Fig. 1 3D infiltration synthetic models (**a**) and a section along an electrode line (**b**)

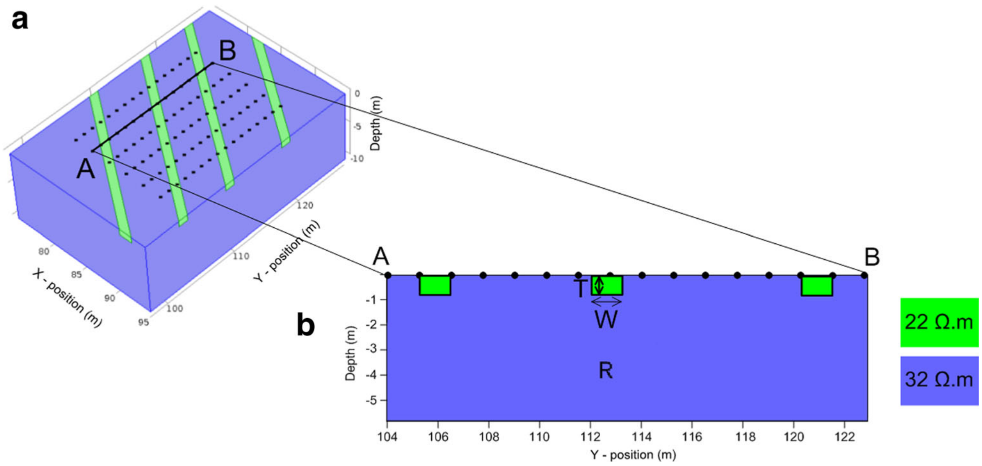

which depends upon the geometry of all four electrodes (Eq. (1)).

$$\rho_a = K \frac{\Delta V_{MN}}{I} \tag{1}$$

To estimate the electrical potential automatically according to the electric current intensity "I" for a quadripole sequence, we used Comsol with Matlab and the F3DM (Forward 3D Modelling) Matlab script (Clement et al., 2011). A Gaussian noise distribution with 3 % standard deviation relative error was added to the apparent resistivity data set to simulate the noise commonly recorded in the field.

3D electrode arrays

Six parallel lines 2.5 m apart were used on the different infiltration models (Fig. 1). Each electrode line included 16 electrodes spaced 1.25 m apart for a total profile length of 18.75 m. A complete sequence of 906 quadripoles was simulated, composed of 534 dipole-dipole quadripoles and 372 gradient quadripoles. Gradient and dipole-dipole arrays allow a multichannel fast acquisition technique. The dipole-dipole array was also chosen for its good sensitivity to the lateral variations of resistivity and it is also widely used in the literature for time-lapse ERT measurements (Clément et al., 2010; Kim and Cho, 2011; Robert et al., 2012).

Inversion

The inversion of the apparent resistivity data sets was performed using BERT software (Günther and Rücker, 2011; Günther, 2004; Günther et al., 2006; Rücker et al., 2006). A finite element method, using tetrahedral mesh for 3D models and triangular mesh for 2D models, was used to solve the forward problem in the routine inversion program (Günther and Rücker, 2011). The "blocky model" option or the L1 norm, which minimizes the sum of the spatial variations in the resistivity model, was used. It is appropriate for significant resistivity contrasts, such as infiltration, and tends to produce models with sharp boundaries (Ellis and Oldenburg, 1994). Isotropic smoothness-constrained regularization and a quasi-Gauss Newton optimization method were used with a fixed regularization parameter ($\lambda = 30$). The anisotropy factor was chosen to correspond to an environment whose electrical resistivity distribution is isotropic (Z weight = 1.0). An option to recalculate the Jacobian matrix at each iteration was also used. BERT software performs inversion combining both electrode array (dipole-dipole and gradient) quadripoles. The time-lapse inversion was performed with a set as reference approach. This approach consists in inverting the initial apparent resistivity model (without infiltration) and then inverting the following time step data set using the initial calculated resistivity model of the initial state as a reference model at the start of the inversion. Finally, we calculated the ratio between the final calculated resistivity model and the initial calculated resistivity model. This is a standard procedure for most time-lapse monitoring to better consider small time variations in resistivity (Loke, 2000).

Field experiment

Measurement area

The experiment was carried out at the Boissy le Châtel plot, part of the GIS ORACLE observatory (Tallec et al., 2015) located 70 km east of Paris (Fig. 2a). The 600 m^2 plot was artificially drained in 1972 by drains placed 6 m apart and connected to a collector which conducts water toward the plot outlet. The plot is described in a previous study by Clement et al. (2014). Each drain is an assembly of pottery pipe tiles with 40 mm inner diameter, 60 mm outer diameter and 30 cm long. Excess water in the soil penetrates into the drain through the joint space between two tiles. The pipe depth is 60 cm laid

Table 1 Variation in the different parameters of infiltration models

Infiltration thickness T (m)	0.3									0.55									0.8								
Infiltration width W (m)	0.4			0.7			1			0.4			0.7			1			0.4			0.7			1		
Resistivity ratio (R)	0.69	0.78	0.89	0.69	0.78	0.89	0.69	0.78	0.89	0.69	0.78	0.89	0.69	0.78	0.89	0.69	0.78	0.89	0.69	0.78	0.89	0.69	0.78	0.89	0.69	0.78	0.89

on a semi impervious clay layer (Fig. 2b). Soil occupation has been permanent grass since tile installation.

Measured profiles of soil moisture are provided by the TDR monitoring system (TRASE instrument from Soil moisture Equipment Corp, Santa Barbara, CA, USA), represented by a green cross in Fig. 2c. The TDR is a measuring method of the propagation time of an electromagnetic wave in a transmission line. In reflectometry, this wave is created by applying a voltage step at the input of a waveguide. In theory, the propagation velocity of an electromagnetic wave V in a medium with a permeability μ_r and dielectric constant ε_r is expressed as follows:

$$V = \frac{C_0}{\sqrt{\mu_r \varepsilon_r}} \tag{2}$$

C_0 is the velocity of light.

In a non-magnetic material permeability, μ_r is equal to 1.

For a discontinuity located at a distance L from the origin of the waveguide, there is an echo after a time T:

$$T = \frac{2L}{V} \tag{3}$$

These equations lead to the fundamental relationship of the TDR signal:

$$\varepsilon_r = \left(\frac{C_0 T}{2L}\right)^2 \tag{4}$$

The volumetric water content θ_V is then calculated using the Topp model standard transfer function (Topp et al., 1980):

$$\varepsilon_r = 3.03 + 9.3\,\theta_V + 146\,\theta_V^2 - 76.7\,\theta_V^3 \tag{5}$$

Where $\theta_V = \frac{V_{eau}}{V_{total.}}$

The device implemented here uses a set of transmission lines consisting of two 20-cm long parallel waveguides, which are horizontally installed. Thus, the device allows obtaining water moisture at different depths in the soil (5, 15, 25, 35, 45, 55, 75, 95, 115, 135 and 155 cm). To validate time-lapse electrical resistivity variations, the electrical resistivity and water content measurements are compared in the next section.

Water injection system

The injection system is composed of a 1-m^3 water tank, connected to the outlet of the collector of the drainage system. Figure 2 shows the whole injection system with the drains and ERT electrode lines. This injection system imposes a constant hydraulic head through a water column 185 cm high using a solenoid valve system coupled with the distribution of network water to provide the refill of the tank, as shown in Fig. 2c. At the bottom of the tank, a pressure transducer (Madofil by IRIS

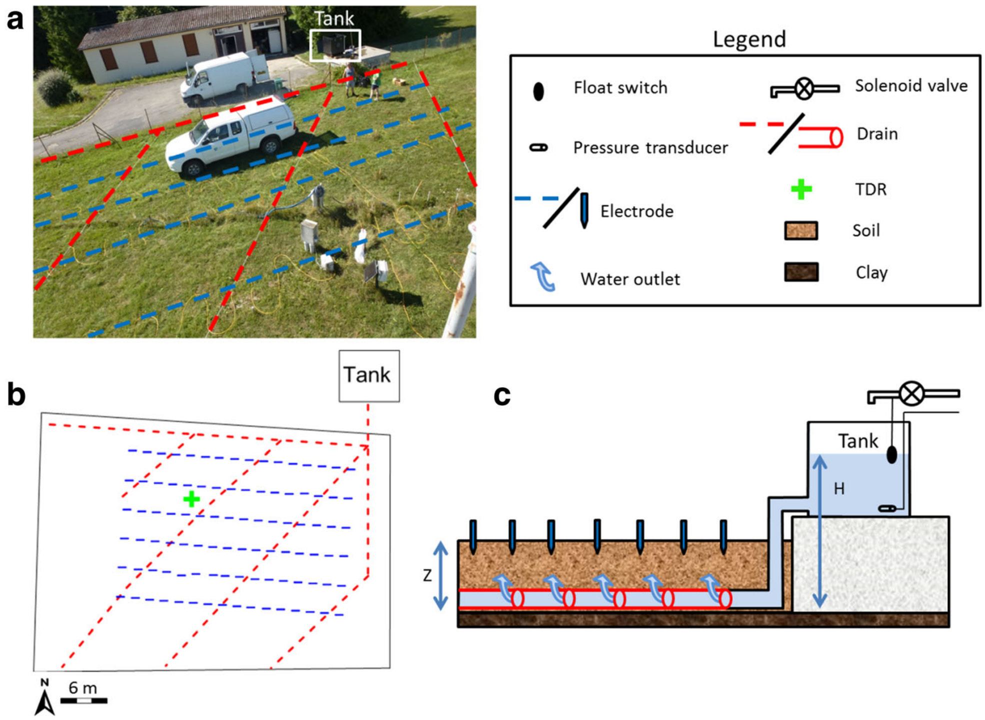

Fig. 2 Field experiment area: **a** location of the experimental site; **b** electrode implantation map; **c** water injection system. *H* hydraulic head (1.85 m)

Instruments, Orléans, France) logs the water level every 15 s to calculate flow and the volume injected.

The tank was first filled to a 40-cm head on August 28, 2013, at 11 a.m. Twenty hours later, when the water injection began, a rapid discharge of the tank was observed in 2 min. The water level then stabilized at 2 cm from the bottom of the tank and rose gradually. Once the tank was filled again with a water column 185 cm high, the water level was maintained at this level. In August 28 at 21:15, a level regulation of the water was started using a solenoid valve coupled to a float switch. Then, the injection system provided a constant hydraulic head on the network drain. The servo system maintained the water level at more or less 1.25 cm, a negligible variation. The water level monitoring in the tank is illustrated in Fig. 3a, c.

Figure 3c shows the flow rate and cumulative volume of injected water monitoring during the experiment. The injection was conducted for about 3 days, from 28 to 31 August 2013. During this period, no rainfall occurred and the injected water flux was constant, except during the discharge of the first 2 min of the injection phase. A total water volume of approximately 60 m^3 was injected over a period of 74 h, representing an equivalent of 100 mm of rain on the experimental plot (600 m^2). The experiment was conducted at the end of August, a period in which the water content of the soil was close to 0.2, corresponding to the lowest values recorded during 2013 (Fig. 4). These values provide the maximum water content contrast and consequently the highest resistivity contrast, as explained above (II.2.).

Electrical resistivity tomography field measurements

Electrical resistivity was measured using a multi-channel resistivity meter Syscal pro (IRIS Instrument, Orléans, France) equipped with 96 stainless steel electrodes. The electrode geometry used on the experimental site comprises six measurement lines spaced 2.5 m apart and included 16 electrodes with 1.25 m the unit of electrode spacing. To compare the resistivity measurements with each other, the electrode was installed and then left in the same position during the entire measurement period.

All electrical resistivities were measured using the same type of electrical arrays presented in the numerical part: a dipole-dipole array with 534 quadripoles and a gradient array with 372 quadripoles. Ninety-nine ERT profiles were acquired for each array over a period of 7 days. The measurements were carried out using the high-speed mode with the following parameters:

- Electrical current injection time, 250 mS (for an 8 min acquisition).
- A 16 min delay sequence.
- A fixed 150 V injection potential (V_{AB}).
- There was a single measurement with no repeatability to average the resistivity value measured or compute the deviation.

Three ERT surveys were carried out before the injection with a 20-min time step between each survey. The apparent resistivity variations between these surveys

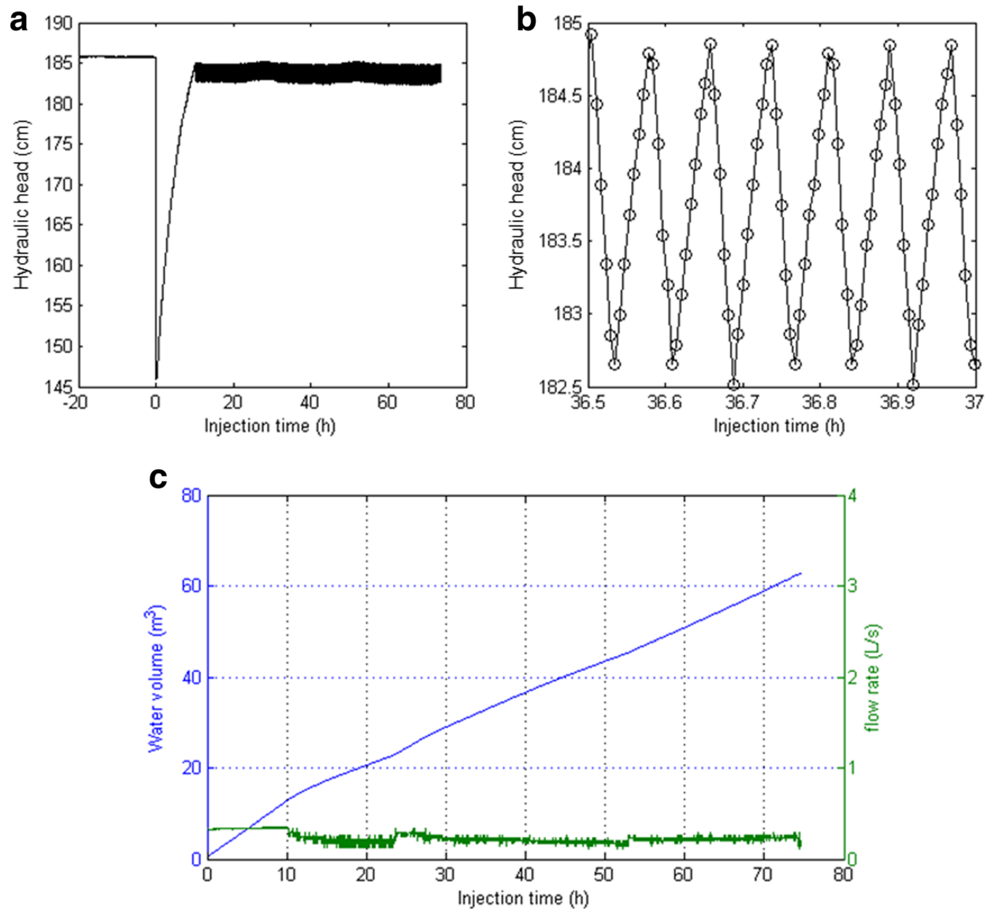

Fig. 3 Water injection monitoring: **a** water injection volume; **b** hydraulic head variation during steady state; **c** flow rate and volume of water injected

were less than 1.7 %, which is why we assume that the electrical resistivity variations recorded during the infiltration process are mainly due to water content variations.

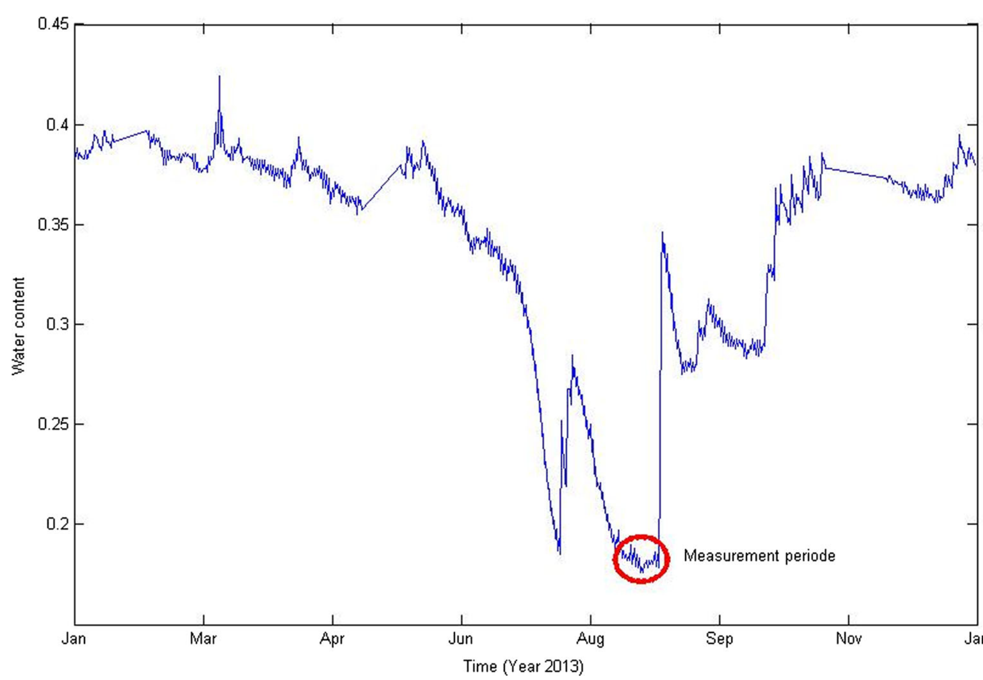

Fig. 4 Water content in 2013 at a depth of 45 cm

Results

Numerical modelling results

Figure 5 presents the results obtained for all numerical models. To facilitate the presentation of 3D calculated resistivity models, the results are illustrated by a selected cross section located under the fifth electrode line, as shown in Fig. 1 (between A and B). We plotted the interpreted resistivity ratio defined by the interpreted resistivity obtained after the injection was divided by the interpreted resistivity before injection. This ratio varied from 0.8 to 1.2. The zones where the ratio was less than 1 (blue, Fig. 5) represent the infiltration area affected by the water injection. Conversely, zones with a ratio greater than 1 (red, Fig. 5) are considered as areas where the water content decreased. While the water content in the wall system cannot decrease during water injection, the increase in resistivity (associated with a water content decrease) is considered as inversion artefacts.

For the entire inversion model, the RMS and Chi^2 values varied, respectively, from 0.2 to 2.5 % and from 0.005 to 0.7. To define the minimal size of an infiltration that can be detected by the ERT, we imposed a simple criterion: when the ratio of the interpreted resistivity is less than 0.9, under one of the electrode lines, the result is considered validated.

In Fig. 5, the black dots represent the electrode position and the rectangles with black contours represent the theoretical infiltration areas. The first infiltration area is located at the left end of the cross sections and centred at 1.8 m. The second one is located in the centre of the synthetic model and centred at 8.9 m. The last one is located at the right end of the cross sections and centred at 16.9 m.

In Fig. 5, in the left part presenting the infiltration with a 0.3-m thickness, whatever the width (from 0.4 to 1.0 m) or bulk resistivity ratio (from 0.89 to 0.69), it can be observed that the interpreted resistivity ratio ranged from 0.95 to 1.05. These ranges of variations are generally regarded as negligible in time-lapse ERT. As long as the infiltration does not have a thickness of at least 0.3 m, no infiltration is detected.

In the centre of Fig. 5, the infiltration with a thickness of 0.55 is presented. The infiltration at the width of 0.4 m, for a bulk resistivity ratio between 0.69 and 0.89, is not detected and the changes in the interpreted resistivity ratio ranged from 0.97 to 1.04. For the infiltration at the width of 0.7 m, there was no change for a bulk resistivity ratio of 0.89 and 0.78. Indeed, the interpreted resistivity ratio ranged from 0.97 to 1.04, which is negligible. In contrast, for the bulk resistivity ratio of 0.69, changes in the interpreted resistivity ratio at different drain positions are more significant (variations between 0.93 and 1.04).

Finally, for a width of 1 m, at the position of theoretical drains, changes in the interpreted resistivity ratio were null for the 0.89 bulk resistivity ratio. For the 0.79 and 0.68 bulk resistivity ratios, the interpreted resistivity ratio decreased less than 0.9. It should be noted that the central infiltration (at position $x = 8.5$ m), located where an electrode is much closer to the infiltration, the interpreted resistivity ratio decreased to

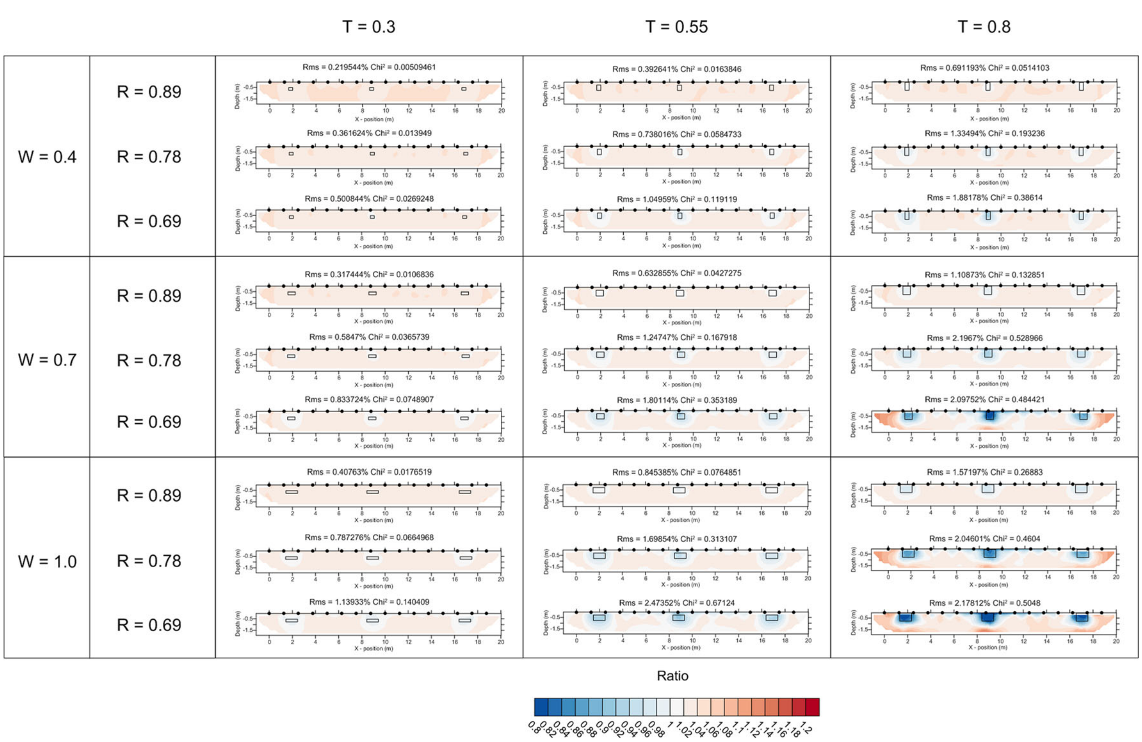

Fig. 5 Cross section extract from 3D time-lapse inversion of synthetic infiltration models

the maximum value of 0.86. For other infiltrations, the variations of the interpreted resistivity ratio were limited to 0.92.

The left part of Fig. 5 presents infiltration with a thickness of 0.8 for a width of 0.4 m, and a bulk resistivity ratio of 0.89 and 0.78. The interpreted resistivity ratio ranged from 0.96 to 1.02, and infiltrations cannot be identified. For a bulk resistivity ratio of 0.69, the infiltration was clearly detected with a decrease in the bulk resistivity ratio to 0.93. For a width of 0.7 and a bulk resistivity ratio of 0.89, no significant interpreted resistivity ratio variation was observed. The same result was observed for a width of 1 m and a bulk resistivity ratio of 0.89. For a width of 0.7 and the 0.78 and 0.69 bulk resistivity ratios, the interpreted resistivity ratio variations ranged from 0.9 to 0.8, respectively. The same results were found for a width of 1 m. For a unit of electrode spacing selected, covering the entire agricultural area studied, it is not possible to increase the unit of electrode spacing if we do not wish to inject much more water into the soil to increase the size of the infiltration area. The infiltration was detected best for thicknesses greater than 0.55 m and a width greater than 0.7 m.

These theoretical results show the limits of ERT, mainly the difficulty detecting small objects on large shallow surfaces. Indeed, to locate drainage pipe, it is necessary to use an electrode spacing unit greater than 1 m to quickly prospect large agricultural plots (>1 ha).

Field experiment results

Based on the numerical results of the previous study, we applied the same unit of electrode spacing (1.2 m) and the same inversion parameters. The aim of the experiment was to validate the detection of infiltration and indirectly the drainage network. Figure 6a shows the measurement of the initial interpreted resistivity before starting to inject water. The interpreted resistivity values varied between 10 and 75 Ω.m. On the 3D block, two shallow areas with the lowest electrical resistivity values were observed, varying between 2 and 10 Ω.m (blue, Fig. 6a) at position $X = 89$ m and $y = 109$ m. These two areas stem from the presence of two metal plates that we could not remove during the monitoring.

Figure 6b presents the ERT measurements; ten major time steps selected are represented of the 99 time steps acquired during the experiment. The resistivity measurements were expressed as an interpreted resistivity ratio defined by the interpreted resistivity at time t divided by the initial interpreted resistivity profile. On this experimental site, the location of the drainage system is well known, because theoretical cartography of the pipe location during its installation in 1972 was available. Drainage pipes were positioned in the 3D inversion model and are represented by red lines at the surface of the 3D model. For each time step, the 3D block presents a threshold, which only retains the interpreted resistivity ratio from 0 to 0.9. On the left part of each 3D model, a slice of the variation of the interpreted resistivity ratio was extracted below electrode line no. 2. The results of the field measurements presented in the Fig. 6 show the following:

(A) The first result of inversion (Fig. 6b) was completed 3 h and 31 min after the beginning of water injection. At this time, 4.7 m^3 of water was injected. The 2D interpreted resistivity slice shows a small variation in the ratio in part of at the theoretical position of the drains ($y = 106$, 113 and 120 m); these variations ranged from 0.85 to 0.9. The 3D model shows a small sector presenting a decrease in the interpreted resistivity ratio (less than 0.9). This variation in soil water content around the drain was not large enough to be identified by the ERT measurements.

(B) After 4h43 (6.2 m^3 of injected water), the interpreted resistivity ratio ranged from 0.83 to 0.95. The drain on the left part of the 3D model was clearly identified with a width of about 0.8 m.

C) Between 5h31 and 6h19, a continuous decrease of interpreted resistivity ratio up to 0.75 can be seen. At 6h19, the location of three major drains was well defined under the true positions of the drained pipes. After 9h31, changes in the interpreted resistivity ratio ranged from 0.7 to 1.2, and the infiltrations around the drain pipe had a respective width (from left to right, Fig. 6) of 0.7, 1 and 0.8 m. At this stage, after having injected 12 m^3 of water, the drains were clearly defined and easily located. Subsequently, changes in the interpreted resistivity ratio gradually rose to 0.65 at the core of the infiltration. There was a progressive increase of the infiltration area but not below 1.2 m. This increase is correlated with soil knowledge of the agricultural plot, including the presence of a clay layer (1 m deep), which probably allows the implementation of a water table or a strongly saturated area around the drain. ERT coupled with water injection was able to locate the drainage network.

Considering the interpreted resistivity ratio observed during water injection monitoring, the pipe network did not seem to be clogged. The growth rate of the infiltration area around drains appeared gradually and continuously during infiltration. We can also consider that the rise in infiltration could be an indicator.

The second drain infiltration size seems to be larger than the other drains. It is likely that this variation of infiltration speed resulted from a different clogging state. The occasional and non-continuous appearance of infiltration at the first times (3h31, 4h43) is probably due to resistivity image reconstruction. These occasional variations were located where the electrode line crosses the infiltration, because at this point, the sensitivity of the ERT measurement is the highest.

Comparison between TDR and resistivity

Both ERT and TDR profile measurements were compared to validate the ERT results. On the experimental site, a TDR

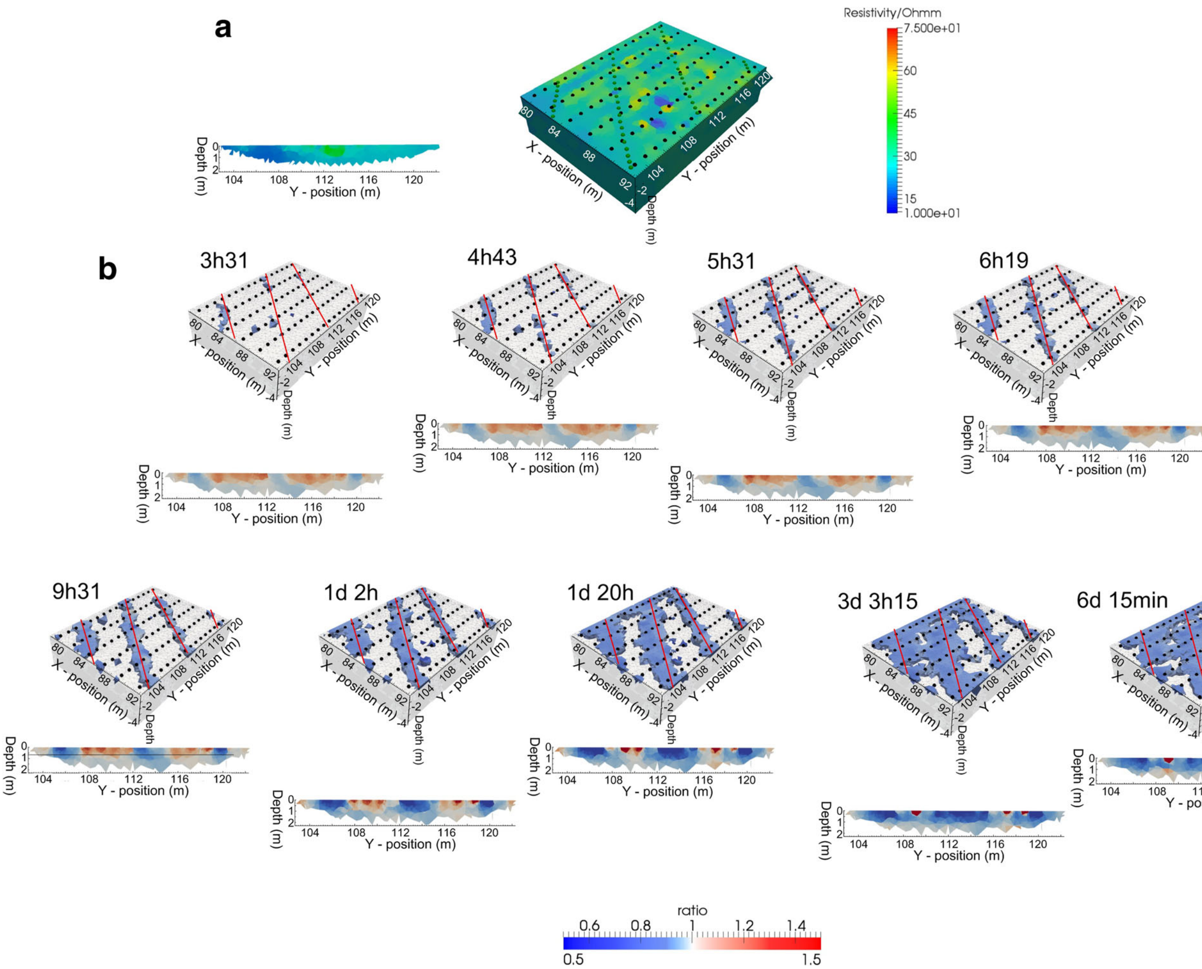

Fig. 6 3D time-lapse monitoring during water injection inside drained pipes: **a** electrical resistivity measurement at initial time step; **b** 3D electrical resistivity monitoring during water infiltration, at several time steps after the beginning of water injection

profile was positioned at the centre of the experimental plot (see Fig. 2). The soil volumetric water content values were derived from TDR measurements. The interpreted resistivity values were extracted from the ERT 3D models presented in Fig. 6 (the closest profile to the TDR sensor) at equivalent depths with TDR measurement. Fourteen TDR and ERT measurement profiles are available for the same times. Given that the electrical conductivity in the soil is proportional to water content, the interpreted resistivity measurements were converted in interpreted conductivity to facilitate the comprehension of the results. The water content and the interpreted conductivity were plotted in Fig. 7 for all time steps and for several depths. Examining the results in their entirety, from the initial state, there is a gradient of water content between the surface and the depth from 0.15 to 0.35. Progressively, during the infiltration processes, the soil water content reached the maximum saturation around 0.35. From the deep layer to the soil surface, a temporal offset of the water content variation was observed. The injection first reached the deeper horizons (from 0.55 to 1.55 m deep, Fig. 7) after 30 h of water injection to reach the more superficial horizons (0.3 and 0.45 m deep, Fig. 7) after 60 h of water injection. The measurement of electric conductivity (ERT) presents a gradient of electrical conductivity with values between 32 and 55 mS/m. The same offset as water content was also observed in the variation of interpreted conductivity. The deeper layers were affected by the infiltration after 40 h and the surface layers were affected after 70 h. The comparison between the ERT and TDR measurements (Fig. 7), for the sensors at 155, 135 and 115 cm deep, shows that the water content was constant and ranged from 0.345 to 0.355.

Discussion

Localizing tile pipes at the plot scale is challenging when they were installed more than 50 years ago. Furthermore, certain pipe diameters cannot be detected precisely with a typical ERT survey. The geophysics technique combined with water injection shows that the resistivity contrast created by the

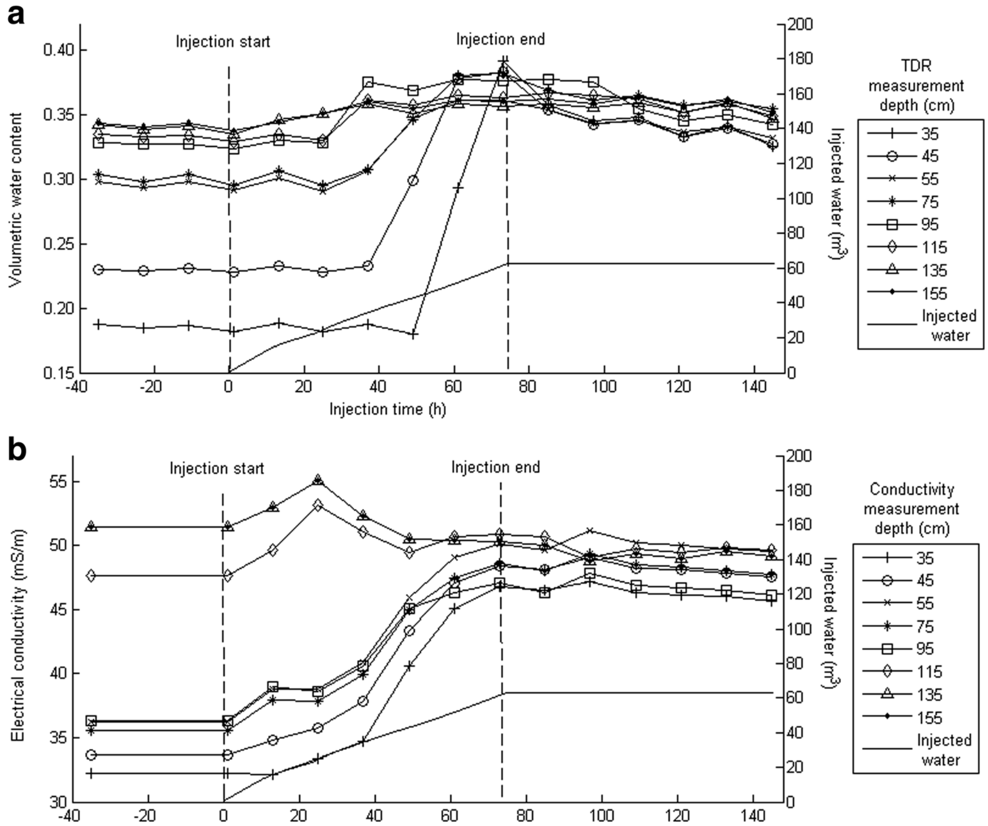

Fig. 7 Monitoring of the water content using TDR measurement (**a**) and the associated electrical conductivity (**b**) over time during the experiment

water injection is strong enough, and then the locations of wet areas correspond to the location of drains. When applied at the field scale in an unknown drainage system, this methodology requires setting the electrode line perpendicular to the main pipe direction (important a priori information). To investigate at a large plot scale, we cannot use complete 3D ERT. Three-dimensional ERT requires many electrodes and a long acquisition time, which is not feasible; we will only use two or three 2D electrical resistivity lines. For future investigations, the injection system also should be designed considering the slope. The methodology used herein is probably not adapted to agricultural plots with a steep slope; in this case, the injection system must be upgraded.

Regarding the injected water volume, the data interpretation showed that to detect soil infiltration using electrodes spaced 1.2 m apart, we must inject 20 m^3 to 200 m^2 to characterize the pipe functioning properly, a large amount of water, but in summer, it can be used to water vegetation. If we consider the variation of electrical resistivity, water fluxes during rehydration are accurately described by the method. The offset of water content variation at different depths (Fig. 7) confirms the behaviour of the drainage system (at a depth of 0.6 m) within the clayey layer located around 0.8 m deep. During the water injection, soil rehydration mainly affects the deeper horizon, after 30 h of water injection, due to gravitational flow. The ERT methodology, compared to local soil moisture TDR measurements, highlights the spatial water flux distribution above and beneath the drainage pipes. To our knowledge, this is the first time that preferential flows beneath a drainage system have been experimentally shown. The clayey layer, generally considered as impervious in modelling approaches (Tournebize et al., 2004) by simplification, allows vertical water fluxes during a transient period of rehydration. Nevertheless, the water rate should be low compared to the annual drainage volume, considering the water content variations (TDR data, 0.34–0.38). Then, when the deeper horizon is saturated, the clayey layer constitutes a temporal impervious layer that allows formation of a temporal perched water table that rises to the surface layers. This can be observed by the increase of soil water content at 0.35 and 0.45 m deep after 60 h. Comparing the variation of interpreted conductivity in these horizons, we observed a lower increase in the interpreted conductivity from 45 to 52 mS/m between 0 and 50 h and then stabilization after 70 h. These changes are non-significant and we assign them to two sources, without being able to verify: either a change in the interpreted conductivity of the solution at the beginning of the injection (cationic exchange) or an ERT inversion artefact. For the other depths, with both electrical conductivity and TDR measurements, the observed variations show similar trends with progressive changes in interpreted conductivity and water content. In conclusion, these results show a good correlation between ERT and TDR measurements in the soil, which confirms and validates the use of ERT for this application. Despite the large unit of electrode spacing used to visualize variations between 0 and 1.5 m deep, the data collected is relevant to measure changes in water contents and then to locate the drainage network.

Conclusion

Location and evaluation of the agricultural drainage networks in the Paris basin is an important economic issue considering the percentage of area drained in the Paris basin (around 80 %). Through this article, we have demonstrated the pertinence of ERT coupled to water injection to locate the subsurface drainage network in small agricultural plots (300 m^2). The location of drainage networks is important because they were set mostly in the 1980s. These networks are beginning to become defective and old, and the drain systems' maps are often lost. To limit the financial costs of repairing the drainage systems, these networks must be located and their clogging state determined.

This numerical study has demonstrated that the use of the ERT model can locate areas impacted by water injection into the drained network (at a depth from 0 to 1 m). However, there are two significant constraints on the use of ERT: (i) the contrast of resistivity tomography (i.e. the initial water content must be low enough to generate a significant change) and (ii) it is difficult to use inter-electrode spacing greater than 1.20 m to cover large surfaces. Indeed, ERT prospecting for the location of drains is needed to investigate large agricultural areas, to detect infiltration.

In the second part of the study, we applied the methodology chosen to an experimental plot. The results were used to (i) localize the buried drains and (ii) highlight the proper functioning of this network with a continuity of water injection along the drains. The results lead us to conclude that the water injection combined with ERT measurement is a good solution to locate drainage systems. However, the drained plot prospected was very small, and applied to larger agricultural plots, 3D time-lapse ERT reaches its limits due to the huge number of electrodes required to cover larger areas. Alternatively, 2D profiles may be used, providing less information and needing a priori knowledge of drain orientation.

Also, considering the electrical resistivity values observed less than 100 Ω.m, the use of frequency domain electromagnetic method (FDEM) to measure the electrical conductivity seems to be relevant. A FDEM measurement (using EM38 (geonic) or the EMP-400(GSSI) equipment) before injection and 10 h after would probably locate the drainage network. This method allows prospecting large surfaces and depth investigations between 0.6 and 1.2 m. Finally, this injection methodology is limited to soil with very small slopes due to the water injection and the volume of water needed.

Acknowledgments This research was supported by the interdisciplinary research program PIREN-Seine and the ANR program CRITEX-EQUIPEX.

References

Allred BJ, Redman JD (2010) Location of agricultural drainage pipes and assessment of agricultural drainage pipe conditions using ground penetrating radar. J Environ Eng Geophys 15:119–134. doi:10.2113/jeeg15.3.119

Archie GE (1942) The electrical resistivity log as an aid in determining some reservoir characteristics. Trans AIME 146:54–62. doi:10.2118/942054-G

Audebert M, Clément R, Touze-foltz N, Günther T, Moreau S, Duquennoi C (2014) Time-lapse ERT interpretation methodology for leachate injection monitoring based on multiple inversions and a clustering strategy (MICS). J Appl Geophys 111:320–333. doi:10.1016/j.jappgeo.2014.09.024

Allred BJ, Daniels JJ, Fausey NR, Chen C, Peters L Jr, Youn H (2005) Important considerations for locating buried agricultural drainage pipe using ground penetrating radar. Appl Eng Agric 21:71–87. doi:10.13031/2013.17915

Allred BJ, Fausey NR, Peters L Jr, Chen C, Daniels JJ, Youn H (2004) Detection of buried agricultural drainage pipe with geophysical methods. Appl Eng Agric 20:307–318. doi:10.13031/2013.16067

Barker R, Moore J (1998) The application of time-lapse electrical tomography in groundwater studies. Lead Edge. doi:10.1190/1.1437878

Bauer-Gottwein P, Gondwe BN, Christiansen L, Herckenrath D, Kgotlhang L, Zimmermann S (2010) Hydrogeophysical exploration of three-dimensional salinity anomalies with the time-domain electromagnetic method (TDEM). J Hydrol 380:318–329. doi:10.1016/j.jhydrol.2009.11.007

Benson AK (1997) Mapping groundwater contamination using dc resistivity and VLF geophysical methods—a case study. Geophysics. doi:10.1190/1.1444148

Braun M, Yaramanci U (2008) Inversion of resistivity in magnetic resonance sounding. J Appl Geophys 66:151–164. doi:10.1016/j.jappgeo.2007.12.004

Brunet P, Clément R, Bouvier C (2010) Monitoring soil water content and deficit using electrical resistivity tomography (ERT)—a case study in the Cevennes area. France J Hydrol 380:146–153. doi:10.1016/j.jhydrol.2009.10.032

Caul-Futy, F., 1994. Methodologie de realisation de plans d'ouvrages anciens en drainage agricole: Comparaison de trois méthodes.

Cazorzi F, Fontana GD, Luca AD, Sofia G, Tarolli P (2013) Drainage network detection and assessment of network storage capacity in agrarian landscape. Hydrol Process 27:541–553. doi:10.1002/hyp.9224

Chaudhuri A, Sekhar M, Descloitres M, Godderis Y, Ruiz L, Braun JJ (2013) Constraining complex aquifer geometry with geophysics (2-D ERT and MRS measurements) for stochastic modelling of groundwater flow. J Appl Geophys 98:288–297. doi:10.1016/j.jappgeo.2013.09.005

Chow TL, Rees HW (1989) Identification of subsurface drain locations with ground-penetrating radar. Can J Soil Sci. doi:10.4141/cjss89-023

Clement R, Bergeron M, Moreau S (2011) COMSOL multiphysics modelling for measurement device of electrical resistivity in laboratory test cell. In: Conference proceedings from European COMSOL conference in Stuttgart

Clément R, Descloitres M, Günther T, Oxarango L, Morra C, Laurent J-P, Gourc J-P (2010) Improvement of electrical resistivity tomography for leachate injection monitoring. Waste Manag 30:452–464. doi:10.1016/j.wasman.2009.10.002

Clément R, Descloitres M, Günther T, Ribolzi O, Legchenko A (2009) Influence of shallow infiltration on time-lapse ERT: experience of advanced interpretation. Comptes Rendus - Geosci 341:886–898. doi:10.1016/j.crte.2009.07.005

Clément R, Moreau S, Henine H, Guérin A, Chaumont C, Tournebize J (2014) On the value of combining surface and cross-borehole ERT measurements to study artificial tile drainage processes. Near Surf Geophys 12:1–14. doi:10.3997/1873-0604.2014034

Descloitres M, Ruiz L, Sekhar M, Legchenko A, Braun JJ, Mohan Kumar MS, Subramanian S (2008) Characterization of seasonal local recharge using electrical resistivity tomography and magnetic resonance sounding. Hydrol Process 22:384–394. doi:10.1002/hyp.6608

Ellis RG, Oldenburg DW (1994) Applied geophysical inversion. Geophys J Int 116:5–11. doi:10.1111/j.1365-246x.1994.tb02122.x

Günther, T., 2004. Inversion methods and resolution analysis for the 2D/3D reconstruction of resistivity structures from DC measurements. University of Mining and Technology, Freiberg (Germany).

Günther, T., Rücker, C., 2011. Boundless electrical resistivity tomography, BERT.User Tutorial.

Günther T, Rücker C, Spitzer K (2006) Three-dimensional modelling and inversion of dc resistivity data incorporating topography—II. Inversion Geophys J Int 166:506–516

Henine H, Nédélec Y, Augeard B, Birgand F, Chaumont C, Ribstein P, Kao C (2010) Effect of pipe pressurization on the discharge of a tile drainage system. Vadose Zo J 9:36. doi:10.2136/vzj2008.0152

Kim K-J, Cho I-K (2011) Time-lapse inversion of 2D resistivity monitoring data with a spatially varying cross-model constraint. J Appl Geophys 74:114–122. doi:10.1016/j.jappgeo.2011.04.010

Lagacherie, P., 1987. Inventaire des sols hydromorphes de France au travers des études préalables au drainage réalisées dans le cadre de l'opération ONIC-MINAGRI-INRA (No. 589). Montpellier.

Lesaffre B (1989) Drainage design practices in France. Irrig Drain Syst 3:181–191. doi:10.1007/BF02576968

Loke, M.H., 2000. Electrical imaging surveys for environmental and engineering studies.

Rogers MB, Cassidy JR, Dragila MI (2005) Ground-based magnetic surveys as a new technique to locate subsurface drainage pipes: a case study. Appl Eng Agric 21:421–426. doi:10.13031/2013.18461

Mathé V, Lévêque F (2003) High resolution magnetic survey for soil monitoring: detection of drainage and soil tillage effects. Earth Planet Sci Lett 212:241–251. doi:10.1016/S0012-821X(03)00241-3

Michot D (2003) Spatial and temporal monitoring of soil water content with an irrigated corn crop cover using surface electrical resistivity tomography. Water Resour Res. doi:10.1029/2002WR001581

Moreau, S., Bouyé, J.M., Barina, G., Oberti, O., 2003. Electrical resistivity survey to investigate the influence of leachate recirculation in a MSW landfill, in: 9th International Waste Management and Landfill Symposium.

Naz BS, Ale S, Bowling LC (2009) Detecting subsurface drainage systems and estimating drain spacing in intensively managed agricultural landscapes. Agric Water Manag 96:627–637. doi:10.1016/j.agwat.2008.10.002

Radulescu M, Valerian C, Yang J (2007) Time-lapse electrical resistivity anomalies due to contaminant transport around landfills. Ann Geophys 50:453–468

Robert T, Caterina D, Deceuster J, Kaufmann O, Nguyen F (2012) A salt tracer test monitored with surface ERT to detect preferential flow and transport paths in fractured/karstified limestones. Geophysics 77:B55–B67. doi:10.1190/geo2011-0313.1

Rücker C, Günther T, Spitzer K (2006) Three-dimensional modelling and inversion of dc resistivity data incorporating topography—I. Modelling Geophys J Int 166:495–505. doi:10.1111/j.1365-246X.2006.03010.x

Samouëlian A, Cousin I, Tabbagh A, Bruand A, Richard G (2005) Electrical resistivity survey in soil science: a review. Soil Tillage Res. doi:10.1016/j.still.2004.10.004

Skaggs RW, Breve MA, Gilliam JW (1994) Hydrologic and water quality impacts of agricultural drainage*. Crit Rev Environ Sci Technol. doi:10.1080/10643389409388459

Tallec, G., Ansart, P., Guérin, A., Delaigue, O., Blanchouin, A., 2015. Observatoire Oracle.

Topp GC, Davis JL, Annan AP (1980) Electromagnetic determination of soil-water content measurement in coaxial transmission lines. Water Resour Res 16:574–582

Tournebize J, Kao C, Nikolic N, Zimmer D (2004) Adaptation of the STICS model to subsurface drained soils. Agronomie 24:305–313. doi:10.1051/agro

Yang J (2005) Geo-electrical responses associated with hydrothermal fluid circulation in oceanic crust: feasibility of magnetometric and electrical resistivity methods in mapping off-axis convection cells. Explor Geophys. doi:10.1071/EG05281

Zimmer D, Lorre E, Lesaffre B (1995) Parameter sensitivity and field evaluation of SIDRA model. Irrig Drain Syst 9:279–296. doi:10.1007/BF00880868